In Vivo Validation of Distributed Source Solutions for the Biomagnetic Inverse Problem

Andreas A. Ioannides*, Robert Muratore#, Marshall Balish†, and Susumu Sato†

Summary: Probabilistic modelling of continuous current sources is applied to the analysis of MEG signals generated by current dipoles implanted in the head of a living human subject. Estimates of the distribution of activity within a circular disk are obtained from signals generated by a single implanted dipole and by a pair of simultaneously active implanted dipoles. The orientation and depth of the disc is determined in advance from the experimental geometry and the measurements. The resulting reconstructions constitute the first in vivo validation of distributed source imaging; they provide a complementary test to earlier works using computer generated data and tests using point source analysis of signals generated by a single implanted dipole. In this work we provide a literal test of spatial resolution by resolving two nearby point-like sources. Temporal resolution is addressed in a de facto manner by imaging at one millisecond intervals. Computer simulations, with controlled amount of noise, are used to demonstrate the robustness of the results, and show the interplay between high spatial accuracy and noise insensitivity.

Key words: Magnetoencephalography (MEG); Inverse problem; Distributed sources; In vivo validation.

Introduction

The rapid evolution in brain imaging has given detailed insight into structural and functional abnormalities accompanying neurological illness. In certain illnesses, in particular in epilepsy, the dynamic aspect is of special importance, and methods such as magnetoencephalography (MEG) and electroencephalography (EEG), which have high temporal resolution, should be of great use (Balish et al. 1989; Baumgartner and Deecke 1990). Recently, methods have been developed that can present dynamically the functional information obtained from MEG (Ioannides et al. 1990a). From a clinical point of view, visualizing the evolution of interictal or ictal discharges might be of great assistance when surgical therapy for epilepsy is contemplated. From a research point of view, such visualization might lead to better understanding of basic processes involved in the generation of such activity. Similar insight might be gained in the study of other illnesses with a fluctuating time course, e.g., migraine and cerebrovascular disease (Tepley et al. 1989), although the electromagnetic field changes have less primacy in the latter illnesses than in epilepsy.

Brain function is based on neuronal activity sustained by the conversion of chemical energy to electrical energy. On a macroscopic level this primary activity acts like a battery impressing a direct current flow (the primary current) which is accompanied by a passive flow of current in the surrounding medium (the volume current). Amongst the various techniques used to study the dynamics of brain function only MEG and EEG are capable of extracting information at a millisecond by millisecond rate relating to the large scale activity of the brain (Ioannides 1991). Detection, sizing and imaging of the primary currents are fundamental goals of both EEG and MEG. In principle a spatiotemporal description in terms of either highly localised sources (e.g., current dipoles) or distributed current density can be extracted from either MEG or EEG signals for both spontaneous as well as evoked responses. However, the expression for the magnetic field (which makes up the MEG signal) contains a part which depends only on the primary current density; the contribution from the conductivity discontinuities introduced by the intervening tissues and bone generate an additional, usually smaller, term, which can be minimised by appropriate design of the experiment. This is in sharp contrast with EEG where the ob-

*The Open University, Department of Physics, Milton Keynes, UK.
#Department of Physics and Astronomy, State University of New York, Geneseo, NY, USA.
†Neurophysiology Unit, Medical Neurology Branch, National Institute of Neurological Disorders and Stroke, National Institutes of Health, Bethesda, MD, USA.

Accepted for publication: October 17, 1992.
This work was done in part while Robert Muratore held a National Research Council/National Institutes of Health Research Associateship. This work has benefited from research grants from the Science and Engineering Research Council (UK), including an award under the Computational Science initiative. Travel assistance to one of us (AAI) from the Nuffield foundation is also acknowledged.

Correspondence and reprint requests should be addressed to A. A. Ioannides, Department of Physics, The Open University, Milton Keynes MK7 6AA UK.

servable, i.e., the surface potential distribution, is strongly influenced by the conductivity of the intervening tissues, including the skull. The transparency of the tissues and bone to the magnetic field has led to an increasing interest in using MEG as a tool to gain insight into basic cerebral mechanisms.

A simple and common model for the biological generators describes the primary activity as one or more current dipole point sources. Effects of the medium and the bounding surfaces of the brain are usually incorporated by assuming that the primary current dipoles are embedded in a conducting sphere of spherically symmetric conductivity. The use of point sources produces a comparatively easy mathematical model and leads to a tractable computational problem. Also, the solution of the inverse problem is easy to understand (a choice for the position and direction of the current dipole(s) which fits the data best), and easy to project onto anatomical landmarks. Recent studies have exemplified how the simplicity of the current dipole model can be used to classify systematically the temporal evolution of brain activity following auditory stimulation around well defined latencies where the signal is strongest (Pantev et al. 1986; Papanicolaou et al. 1990). In these studies the evolution of the current dipole parameters must be viewed as a reflection of the average behaviour of neuronal populations which may have an appreciable spatial extent (Hoke et al. 1989). Difficulties sometimes arise with the multiple dipole model because superposition of the sources can lead to an arbitrary choice of the number of model dipoles (Balish et al. 1991).

Distributed source solutions have been proposed by a number of authors (Hämäläinen and Ilmoniemi 1984; Kullman et al. 1989; Crowley et al. 1989). We will use the distributed source method developed at the Open University (Ioannides et al. 1990a; Ioannides et al. 1990b) which is based on probabilistic treatment of continuous current sources (Clarke and Janday 1989; Clarke 1989). The resulting distributed solutions provide a novel view, dispensing with idealized dipolar points in favor of a probability distribution which is interpreted as an estimate of the electrical current density underlying the measured magnetic fields.

Results from distributed source analysis of in vivo measurements of natural sources, from both evoked responses or spontaneous activity, have already been reported (Ioannides et al. 1989a and 1990b; Ribary et al. 1991), including comparisons of solutions obtained using three dimensional distributed models and current dipoles (Ioannides et al. 1993). Despite the fact that these works provide indirect support, the underlying sources are insufficiently characterized to provide a clear, unambiguous test. However, there are measurements of the neuromagnetic field generated by well-characterized in vivo sources, namely, dipole-like sources implanted in a patient's head (Rose et al. 1989a; Rose et al. 1989b; Balish et al. 1991). A comparison of the inferences drawn from these measurements provides an important validation of the distributed source method under controlled yet realistic conditions. However, these tests have their own disadvantages, arising from the overriding need to minimise patient discomfort and associated practical constraints. In dealing with in vivo data generated by the implanted sources, which are not related to immediate clinical needs, we have to accept instrumental and other uncertainties which are far more serious than similar problems encountered in other research and clinical settings. Given these limitations and the fact that we had data from only one subject we have complemented the in vivo analysis with analysis of computer generated data.

Methods

Data Collection

We have studied one patient with intractable partial epilepsy who had subdural electrode monitoring for localisation of seizure focus. Procedures were discussed in detail and informed consent obtained. Specially designed dipolar electrodes (Rose et al. 1989a) were implanted at selected locations. The patient was brought to the MEG lab where selected dipoles and dipole pairs were studied.

All recordings were performed in a shielded room using a 7 channel (DC-Squid based) neuromagnetometer with second order coil configurations (Biomagnetic Technologies Inc. (BTi) model 607), coil diameter 15.1 mm and baseline 40.4 mm. Data were digitized and analyzed on a Hewlett Packard HP 9000/series 300 computer using commercially available software (BTi); filter settings were 0.3 Hz high pass and 1000 Hz low pass with 24 dB/octave roll-off, and the sampling rate was 1024/sec per channel. The high value of the low pass filter frequency minimizes distortion of the square waveforms which drive the implanted dipoles. There is a resulting inconsistency in the choice of sampling rate and filter parameters, but since the experiment can only be repeated on clinical grounds we must make the best of the available data. The frequency spectrum above 200 Hz, shows little activity, aside from what appears to be very attenuated noise. It appears that the violation of Nyquist theorem results in some unnecessary aliasing, which apart from lowering the signal to noise ratio, it has no bearing on our conclusions.

Head shape and probe positions were determined with the probe position indicator (PPI device, BTi). The patient was positioned on a wooden bed lying on the side opposite the dipole(s) of interest and the probe was posi-

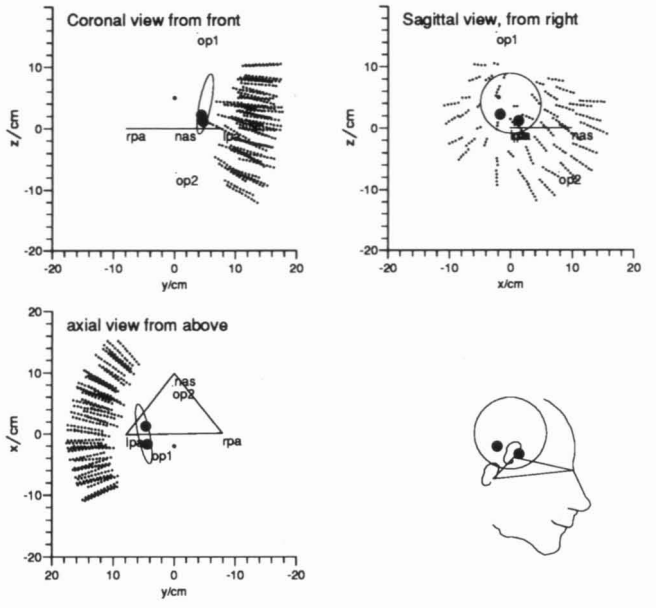

Figure 1. Coronal (top left), Sagittal (top right) and axial (bottom left) views of the coordinate system and experimental arrangement. A dotted line shows the line connecting the centres of the three sets of coils for each gradiometer. The left and right pre-auricular points (lpa and rpa) and the nasion (nas) are marked on the diagram and they are connected by a line to form a triangle. The locations of the two implanted dipoles are marked by a heavy dot, while the centre of the conducting sphere assumed in the inversions is marked by a light dot. The circle in each diagram shows the boundary of the source space used in distributed source analysis. The diagram on the bottom right shows a nearly sagittal view together with a sketch of the face profile and ears. This view will be used to show contour plots of the signal (figure 2) and to display distributed source solutions (figures 4-6). The triangle formed by joining lpa, rpa and nasion will be drawn on all figures as an orientation aid.

tioned almost touching the patient's head. The probe was sequentially moved over a grid of points (see figure 1). The full set of data was obtained from 11 probe positions yielding 77 channels of data in total from which the extrema of the magnetic field plots could be defined. The repetition of the dipole activation for each probe position presents no problem in our experiments. The corresponding repetitions in evoked response studies is problematic because of non-stationarity effects. However, the introduction of multichannel facilities with 37 or more channels has now eased considerably, but not entirely eliminated, this problem.

Two sets of signals will be considered in this paper; each set consisted of 77 time series, one for each channel, obtained by averaging 200 epochs. Each epoch contained 150 time slices separated by 1 millisecond. The probe relocation under the conflicting needs to cover with sensors a sizeable part of the head and at the same time to minimize patient handling time produced some nearly coincident sensor locations. The inclusion of signals from closely spaced sensors has two undesirable effects: it increases computation time and it generates instabilities (which however can be easily eliminated using standard mathematical techniques, e.g., singular value decomposition). We have avoided both these problems by using 49 of the 77 time series, corresponding to 49 channels selected on purely geometric considerations (they are well separated from each other). There is practically no change in the solutions if a few more or less channels are used as long as no nearly coincident channels are included. The signal of interest, within each epoch, was generated by passing a pulse of 40 [mu]A of 5 ms duration through the implanted dipole(s), first in one direction followed by an identical pulse but with the opposite phase 40 ms after the onset of the first one. The first set was generated by activating, in the manner just described, a single implanted dipole, while the second set was generated by activating synchronously both implanted dipoles. Figure 1 shows the head-centre coordinate system, and the relative positions of the head landmarks and implanted dipoles (marked as heavy dots) with respect to the sensors. A pair of Grass S8800 constant current stimulators were triggered by the Hewlett Packard computer. Current density met safety guidelines (Smith et al. 1983, Smith et al. 1985).

In figure 2 the average signal traces from two channels are displayed, with contour plots of the spatial distribution of the signal at time points corresponding to the activation of the dipole(s). Both the signal due to a single implanted dipole and the signal due to a pair of implanted dipoles were fitted to a model incorporating a single dipole source in a spherical head with the inclusion of volume currents. The results for the current dipole location thus derived will be compared with the extended source analysis below.

The coordinates of the implanted dipoles were estimated from skull radiographs obtained with the electrodes in place; the direction of the current flow could not be determined from the radiographs. Care was taken to minimize magnification when taking these x-ray films; the overall location error from the radiographs is estimated to be $\pm$ 0.2 cm.

In the radiographs the images of additional radio-opaque markers attached to the fiduciary points were visible. These markers were used to match the X-ray and MEG co-ordinate systems, and helped in establishing the head centred MEG coordinate system, used for data collection. The origin of the MEG coordinate system was defined as the midpoint of the line joining the pre-auricular points. The positive x axis was defined as the line from the origin

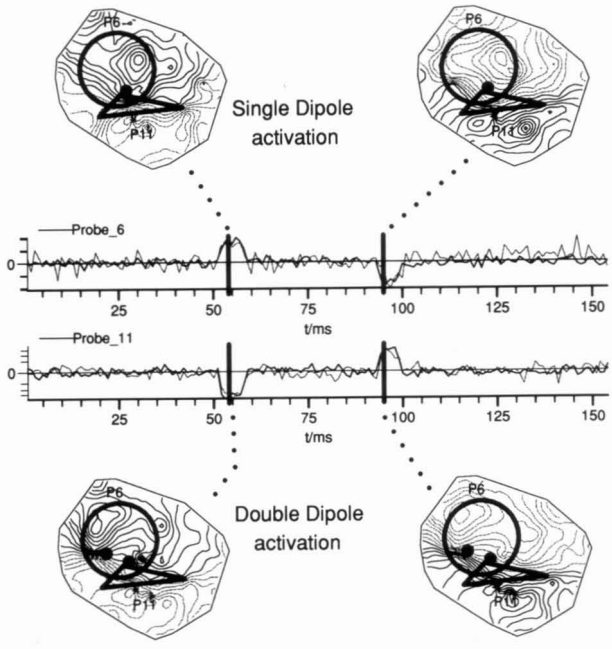

Figure 2. The middle part of the figure shows traces of the magnetic flux recorded by the mid channel of probes 6 and 11. The light dashed (solid) trace in each case corresponds to the signal generated by the activation of one (both) implanted dipole(s). The pair of contour plots above (below) the signal traces shows the distribution of magnetic flux when one (both) implanted dipoles are switched on; the precise latencies are marked by the heavy vertical lines in the signal traces. The magnetic field strength varies from approximately 400 to -400 fT (solid contours are positive and dashed contours negative). The contour plot plane is the nearly sagittal view of the bottom right diagram in figure 1. The circular boundary of the source space and the projection of the lpa, rpa and nasion triangle are marked by heavy circle and triangle respectively. The heavy dots and the symbols P6 and P11 indicate the projections of the implanted dipole(s) and centres of probes 6 and 11.

to the nasion. The z axis was the vector normal to the plane which included the origin and fiduciary points (positive towards the top of the head), and the y axis was perpendicular to the other two axes and positive to the left. The experimental arrangement, coordinate system and important landmarks are depicted in figure 1. The fiduciary points, left and right pre-auricular, and nasion are marked as lpa, rpa and nas respectively, and connected by lines into a triangle. This triangle is printed in all figures as an orientation aid.

Modelling

Two main alternatives to the single dipole model have been developed, multiple dipole models and fully distributed models. Multiple dipole models use the full spatiotemporal variation in the signal to extract estimates for the coordinates of point like equivalent generators. In addition to the original model developed by Scherg and collaborators (Scherg et al. 1985, 1989; Scherg 1990) elaborate methods have been recently developed (Mosher et al. 1990) using a scanning procedure for multiple directional emitters (Schmidt 1986).

In discussing distributed models it is useful to think in terms of the sensitivity profiles of the sensors, or lead fields; this concept was introduced into the biomagnetic source localisation problem by Tripp (Tripp 1983). Hämäläinen and Ilmoniemi (1984) made the explicit suggestion of using the lead fields as an expansion basis to construct distributed current sources. In its simplest form, this procedure leads to biological generators which are as widely dispersed as possible and they have the minimum power sufficient to fit the MEG or EEG signal. A number of such "minimum norm" methods have been proposed recently (Kullman et al. 1989; Crowley et al. 1989). The straightforward implementation of these methods leads to fragile algorithms which even in the absence of noise and other uncertainties can produce only solutions with little detail. It is inconsistent to allow an unrestricted range of "minimum norm" solutions and to demand an exact fit to the signal. This combination either generates a poor solution or, in fitting noise components, introduces unphysical features into the solutions.

Recent works (Clarke and Janday 1989; Clarke 1989; Ioannides et al. 1990a; Ioannides et al. 1990b) have shown how these and other difficulties can be tackled within a probabilistic treatment of the current density distribution. A full description of the resulting method, including a concise description of the algorithm and numerous tests with computer generated data is given elsewhere (Ioannides et al. 1990a). More recently (Ioannides 1991) the method has been contrasted with other modelling approaches which although fundamentally different in nature, have all been referred to, at one time or other, as current density imaging. In the remainder of this section we provide a non-mathematical summary of the method.

A key feature of the method is that it provides an approximate and robust rather than an exact and highly sensitive fit to the data which takes into account the noise content in the measurements; this is achieved by limiting the maximum current modulus so that it is within physiologically feasible limits (Clarke and Janday 1989; Clarke 1989; Ioannides et al. 1990a; Ioannides et al. 1990b). Mathematically, the precise compromise between spatial resolution and stability is determined through a regularisation parameter $\tilde{\zeta}$ which forces the *a priori* probability distribution of the current density to have a finite standard deviation. Large values of $\tilde{\zeta}$ limit

the maximum magnitude of the current density leading to an approximate fit to the data which is rather insensitive to noise (Ioannides et al. 1990a). A small value for $\tilde{\zeta}$ produces an accurate fit by allowing large values for the current density modulus; if the signal to noise ratio is low then the solutions for small $\tilde{\zeta}$ values may be dominated by the noise in the measurements. The appropriate value for $\tilde{\zeta}$ can be determined from the maximum physiologically acceptable current density modulus and the standard deviation of the noise component in the data. In real life however reliable estimates for the maximum current modulus and/or the standard deviation of the noise are not always available. A reasonable value for $\tilde{\zeta}$ can be obtained empirically from the observation that the onset of instability is fast: repeated inversions are performed with the value of $\tilde{\zeta}$ lowered each time, until a critical value where small changes in $\tilde{\zeta}$ produce large changes in the solution. In this as in all earlier works with real MEG data we have used this method for choosing $\tilde{\zeta}$, always erring on the side of caution, by choosing a $\tilde{\zeta}$ value well above the critical value.

The choice of lead fields, as bases for the current density expansion, is maintained, but an overall *a priori* Gaussian shaped, probability weight is introduced so that the bias towards superficial sources is neutralised. In recent works (Ioannides et al. 1989a, 1990b and 1993; Ribary et al. 1991) we have consistently used a Gaussian probability weight, centred at the centre of the conducting sphere; thus the only parameter of the *a priori* probability influencing the inversions is the decay constant of the Gaussian. This parameter is fixed (before the analysis of the signals) so that test sources (usually current dipoles), placed at different places in the source space are correctly reproduced from computer generated data.

Resolution is further enhanced by a rapidly convergent iterative scheme which can consistently recover both distributed activity as well as highly localised activity (Ioannides et al. 1990a). The resulting method is computationally very intensive, and it has been implemented on both the VAX cluster at the Open University, as well as on a dedicated transputer array.

The imaging system can recover either the primary current density with the currents fully accounted for by the conducting sphere or some other model, or it can image the full current density, i.e., the sum of the primary current density and the induced current density from volume currents (Ioannides et al. 1990a). The latter method has advantages in situations where the geometry of the medium is rather complicated and hence difficult to model. Note that the source space defines the region of space within which the primary activity resides. An independent definition is needed to specify the nature and the shape of the conducting medium; for example, the coordinates of the centre of the conducting sphere must be specified if the uniform conducting sphere model is to be used. Finally, a subsystem of the full system is used for point source inversions.

The method produces as solution a continuous probability distribution confined to a well defined source space, which depends on the orientation of the primary current density vector. The relative value of this probability distribution at each point in the source space, and for each orientation is identified as an estimate of the local current density vector. The source space can be along a one dimensional curve (e.g., a line), or a two dimensional surface, (e.g., a disk) or a full 3 dimensional region which in principle follows the shape of the brain exactly. The choice of what source space to use should take into account the sensitivity inherent in the choice and position of sensors and the noise in the data (Ioannides 1991). In typical MEG experiments the sensors are distributed on a surface (which we will call the measurement surface) which follows the rough outline of the head. In the present case gradiometers are used with their symmetry axis perpendicular to the measurement surface so that the contribution from return currents in the signal is minimised. This sensor arrangement, and in particular the fact that the measurement surface covers only a fraction of the head surface, endows the measurements with a much higher sensitivity to source variation along lateral directions rather than directions perpendicular to the measurement surface. In recent 3D inversions (Ioannides et al. 1989a, 1990b, 1993; Ribary et al. 1991) a cylindrical source space has been used, with the lateral surface of maximal sensitivity corresponding to the top face of the cylinder, closest to the sensors. Given the sensor arrangement used in the present experiment, and the additional noise problems introduced by the patient preparation we have restricted the source space to a flat circular disk. Before the data are analysed the centre and orientation of the disc is fixed, independently of the signal, so that it faces the sensor array. Thus, by the time the analysis of the signals begins there remain no adjustable parameters.

The depth of the circular disc, defined as the average distance from the measurement surface (or equivalently the scalp) is estimated using a simple procedure (Ioannides et al. 1990a, 1990b): the standard deviation between the measured signal (for single dipole activation) and the signal produced by the distributed source solution is computed for successive depths. The point where the resulting plot of standard deviation versus assumed depth has a minimum is used to fix the depth coordinate. The same depth is used for the distributed source solutions and simulations for single and pair dipole activations. The circular boundary of the source space (after depth adjustment) is shown in the different views of the experimental arrangement in figure 1.

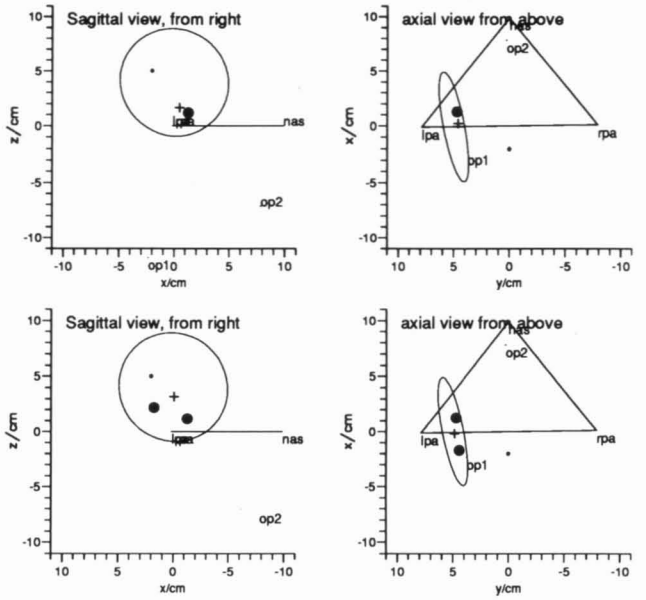

Figure 3. Sagittal and Axial views of the solutions for single equivalent current dipole in a conducting sphere. The top diagram shows the solution for the data generated by the activation of a single implanted dipole. The lower diagram shows the single equivalent dipole solution for the data generated by the activation of a pair of implanted dipoles. The position of the single equivalent current dipole solution is marked by a cross. All other symbols have the same definition as in figure 1. Note that the source space outline is not relevant to the current dipole method, but it is included in the figure to aid comparisons with later figures.

Results

Single Current Dipole Solutions

Before we describe the reconstructions with distributed source models we indicate for later comparison how a single point source model works for these data. The upper part of figure 3 shows the position of the best fit dipole (marked by a cross) when the target signal is generated by a single implanted dipole. These results were obtained using the biomagnetic imaging system at the Open University, in point source recovery mode. All point source parameters were allowed to vary, including the coordinates of the conducting sphere centre. The lower part of figure 3 shows the position of the single equivalent dipole (marked again by a cross) obtained from the data generated by the simultaneous activation of the pair of implanted dipoles. The single equivalent dipole model fits the data in each case reasonably well. The position(s) of the assumed current dipole(s) are shown by the heavy dot(s). A more sophisticated multiple dipole algorithm is likely to perform better in the second case where two implanted dipoles were activated together; no such algorithm is discussed within this work; we wish to evaluate the effectiveness of distributed source solutions with as little constraints as possible in the form of the solutions.

Distributed Source Analysis I: Simulated data

In the remainder of this paper we will consider distributed source models. The primary current density is confined within a circular disc of radius 5 cm. The position and orientation of this disk is determined prior to the distributed source analysis of the signals as described in the last section. The conducting sphere model was assumed in all distributed source analysis. We will present the distributed source solutions either as arrow maps or intensity contour plots. It is important to realise that the solutions are continuous vector functions, confined within the circular disc source space. The arrows in the arrow maps correspond to the local current density vector, sampled at regular points in the source space. The intensity contour plots display the square of the current density modulus.

Following the analysis of the real data (to be described in the next subsection), two sets of simulated data were generated by the computer, so that the distributed source analysis could be studied under controlled conditions. The first set of simulated data was generated by assuming a single current dipole, while the second set was produced by assuming a pair of dipoles. The dipole location(s), sphere centre, sensor type and sensor distribution in space were identical to those in the real experiment. The direction of the current dipoles (which were not determined from the radiographs) were chosen to be similar to those obtained from the analysis of the real signals.

Figure 4 shows the distributed source estimates, obtained from noise free simulated data. Arrow maps of the estimates of the continuous current density are shown in the top figures, while the figures at the bottom display shaded contour plots of the intensity (square of the current density modulus). The group of four figures on the left is obtained from data generated by a single current dipole, while the group of four figures on the right shows identical graphs obtained from data generated by a pair of current dipoles. Within each group the leftmost figures are obtained with $\tilde{\zeta} = 0.05$ while the ones to their right use $\tilde{\zeta} = 0.001$. The first value is large enough to tolerate the level of noise in the actual MEG experiment.

In figure 5 we show identical reconstructions when 15% random noise, somewhat larger than that in the real experiment, is added to the computer generated data. The higher value for the regularisation parameter ($\tilde{\zeta}$ =

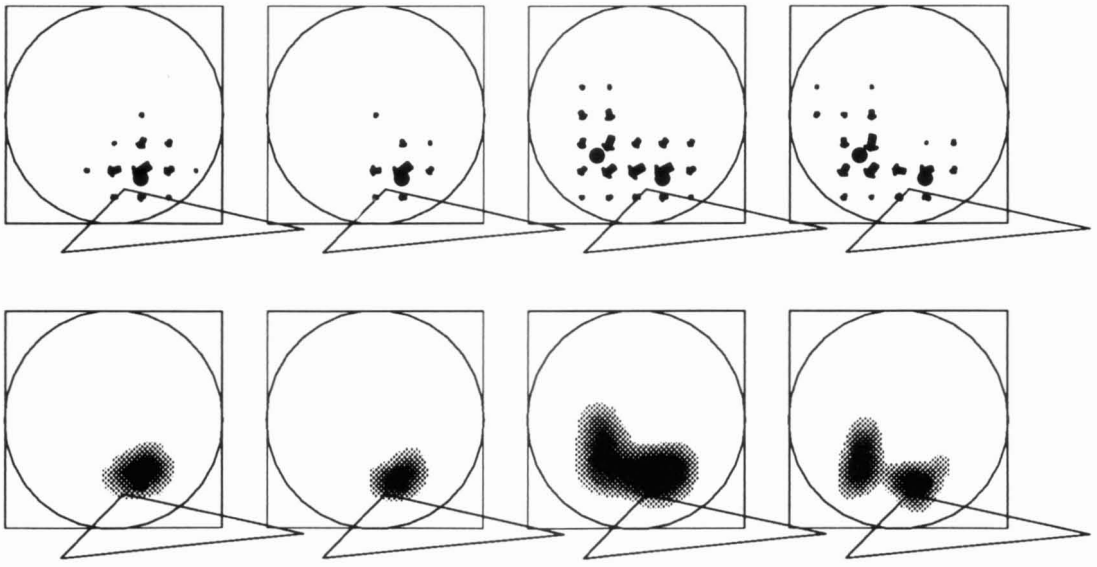

Figure 4. Reconstruction of primary current density from noise free computer generated signals. The signal for the figures on the left is generated by a single point source, while for the ones on the right are generated by a pair of point sources. For each case reconstructions with two different values for the regularisation parameter are shown. The top figures show an arrow map of the current density, while the bottom figures show contour plots of the intensity. The triangle connecting the pre-auricular points and nasion is included to help orientation.

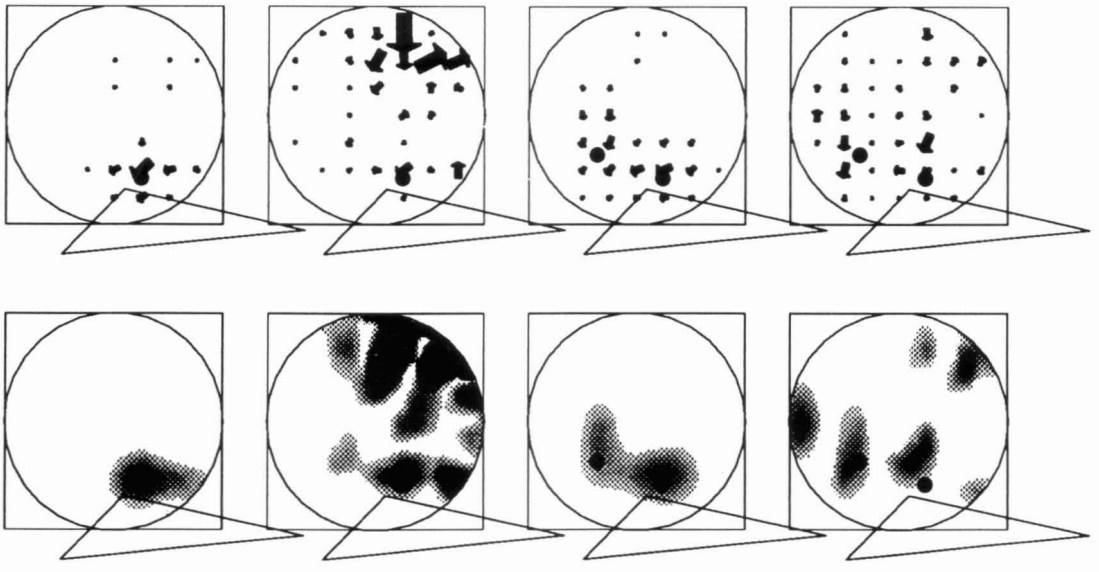

Figure 5. Arrow maps of the current density and contour plots of the intensity for the same computer generated data as in figure 4, but with 15% random noise. All inversion parameters (including the $\tilde{\zeta}$ value) in each column of this figure are the same as the ones used in the inversions of the corresponding column in figure 4. The second and fourth column demonstrate the instability incurred when the value for the regularisation parameter ($\tilde{\zeta} = 0.001$) is too small to cope with the noise in the data.

0.05) is just enough to cope with the level of noise in the data. The resulting estimates are very similar to the ones obtained from noise free data and the same $\tilde{\zeta}$ value, demonstrating the robustness of the method. The reconstructions of noisy data with an inappropriately small value ($\tilde{\zeta} = 0.001$), in the second and fourth column of figures, demonstrate the catastrophic consequences of the resulting instability.

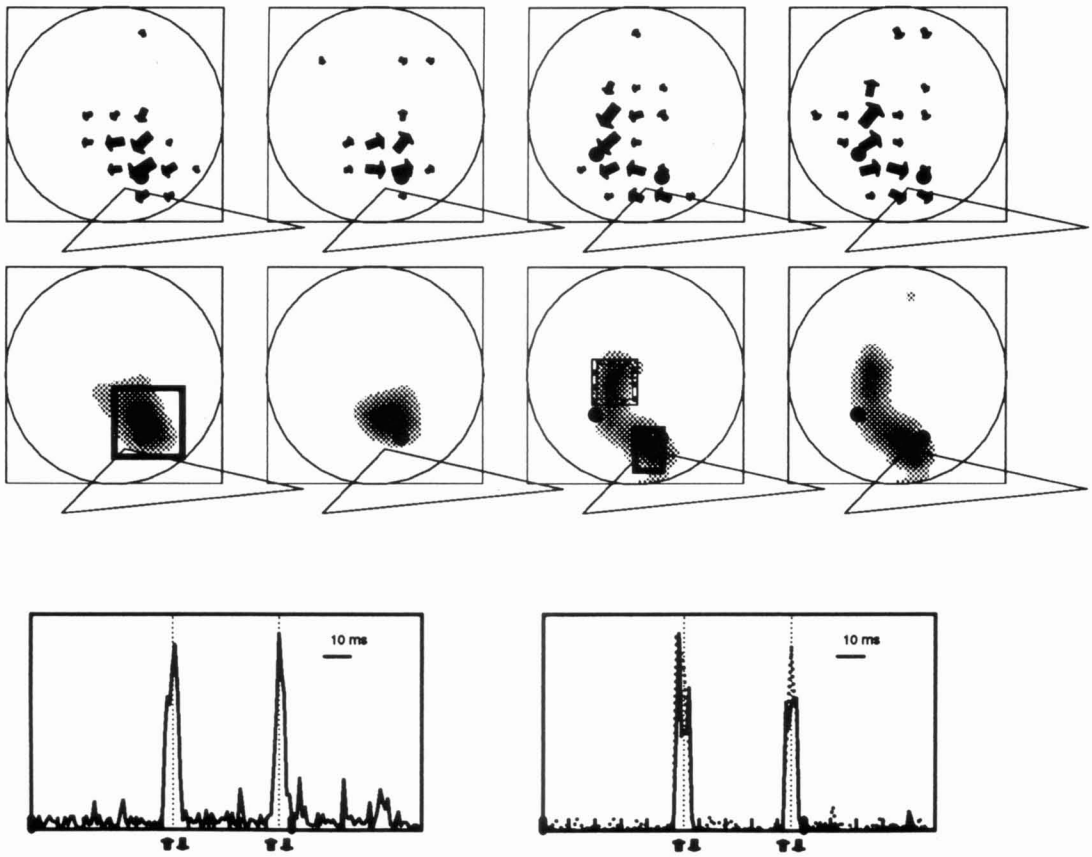

Figure 6. The group of figures on the left (right) show the distributed source solutions for the MEG signals from a single (pair of) implanted dipole(s). For each experiment reconstructions at two latencies are displayed, 40 ms apart, and occurring in the middle of each activation phase. The top row shows the current density vector in arrow map form, while the middle figure shows the corresponding intensity distribution. In all inversions in this figure the value for the regularisation parameter was $\tilde{\zeta} = 0.05$. The position(s) of the implanted dipole(s) and the rpa, lpa and nasion triangle are also shown, in the same way as in previous figures. In the bottom part of the figure the temporal variation of the average intensity within the boxed areas are displayed for the entire 150 ms interval. In the activation plots in the bottom part of the figure, the time slices corresponding to the arrow map and intensity contour plots are marked by a dashed vertical line; also, an up (down) arrow marks the onset (offset) of each 5 ms long activation period for the implanted dipole(s).

Distributed Source Analysis II: In vivo tests

We now turn to the distributed source solutions of the actual signals generated by the implanted dipole(s). The estimates for the single implanted dipole activation (left) and the pair of implanted dipoles (right) are shown in figure 6. A shaded contour plot (middle row) shows the spread in the area of high probability estimate, while the arrow maps (top row) show the direction and relative magnitude of the local current density vector. For each case the solutions in the middle of each phase of source activation is displayed, obtained with regularisation parameter $\tilde{\zeta} = 0.05$. In the bottom part of figure 6 the temporal evolution of the intensity, within the boxed area(s) above is plotted for the entire 150 ms interval.

At the latencies displayed, the estimates for the pair activation show two areas of activity with maxima reasonably close to the locations determined by the radiographs. The images produced at other latencies are similar; in some instances one or other of the two sources appears weak. The direction of the current density is consistent in all latencies within each activation, reversing during the second phase of the activation as the polarity of the implanted dipoles is reversed.

Table 1 provides a concise, albeit oversimplified, summary of the analysis of the implanted dipole data. In this table estimates for the locations of the two sources are given, corresponding to the radiograph determination and the estimate from the single current dipole model. In addition, we also quote the location of where the dis-

Table I. Estimates for the coordinates of the implanted dipoles determined from radiographs and single equivalent current dipole model. The rows marked as DSS max give the coordinates of the centres of regions corresponding to clear maxima in contour plots of the distributed source intensity probability estimates.

Localisation method	Active source	Position coordinates (m)			error (m)
		x	y	z	
Radiograph	1	0.013	0.047	0.012	± 0.002
Radiograph	2	-0.013	0.047	0.022	± 0.002
Single ECD	1	0.005	0.047	0.019	0.011
Single ECD	1 + 2	0.000	0.049	0.034	
DSS max	1	0.013	0.048	0.018	0.0061
t = 54 ms					
DSS max	1	0.007	0.047	0.020	0.010
t = 95 ms					
DSS max	1 + 2	0.007	0.045	0.008	0.007
t = 54ms		-0.011	0.047	0.037	0.015
DSS max	1 + 2	0.006	0.045	0.08	0.008
t = 95ms		-0.011	0.047	0.038	0.015

tributed source solution estimate exhibits a pronounced maximum.

Discussion

There are several limitations in this experiment, in addition to the inconsistency between filtering parameters and sampling rate. First, although we have assumed a spherical conductor, the skull is not truly spherical and the departure from sphericity is perhaps most pronounced in the temporal regions where the sources were placed and measurements performed. Second, although the source design was carefully considered, these electrodes were being used to obtain clinical information as well as to serve as current sources. The interpole distance was finite (5 mm), which is a departure from an infinitesimal current source. In addition the silastic support interrupts volume currents although the size of the support was kept to a minimum and the platinum contacts were exposed on both sides (Rose et al. 1989a). Third, since our patient had undergone craniotomy for placement of electrodes, there was soft tissue swelling and it was necessary for him to wear a somewhat cumbersome bandage which kept the probe up to 2 cm farther from sources than otherwise would have been the case. Therefore the measured signal was reduced. In addition there may have been some contribution to noise from sources such as the implanted electrodes (125 over the left hemisphere), associated wires, connectors and recording equipment used to monitor the patient and the stainless steel staples used to close skin incision.

Despite these limitations, the distributed source solutions have produced good descriptions of the activity, with accuracy almost as good as the one obtained from simulated data. The probability estimates exhibit pronounced maxima close to highly localised activity, and the direction of the current flow was constant during each 5 ms activation interval. The direct comparison in table 1, between the locations of the maxima and the coordinates as determined by radiographs gives too flattering a picture. We prefer to work under the assumption that the distributed source solutions have an inevitable spread, as demonstrated by the solutions with computer generated data; for typical MEG measurements this is in the order of about 0.5 cm. The advantages of distributed source models lies not in precise localisation of point like activity, but in accurate description of the activity without drastic *a priori* assumptions about its shape. It is of course impossible to produce a truly distributed in vivo test using just a few implanted dipoles. However, extensive tests with computer generated data have shown that the method works much better for truly distributed source configurations (Ioannides et al 1990a).

We have consistently used a circular disk as source space and we have determined the depth of this disk below the measurements in a very simple way. The method is very flexible and more elaborated choices for the source space could have been made, exploiting additional information. This has proven unnecessary since the position of both the single and double implanted dipoles were recovered with reasonable accuracy using this simple choice of source space. The orientation of the source space disc was fixed in terms of the sensor arran-

gement, and the depth was determined through a simple procedure; the inaccuracy in the depth determination accounts for much of the error in the distributed source analysis, particularly for the second source in the pair activation.

The analysis so far was restricted to producing static images at fixed points in time. The activation curves in figure 6 show a glimpse of what can be displayed. The power of our imaging system is fully exploited when such images are put together into animated sequences. A number of MEG signals arising from visual auditory evoked responses have been analysed in this way (Ioannides et al. 1990b) and the results recorded on video (Ioannides et al. 1989b).

The animations produced from the data presented in this paper show a seemingly random brain activity, until the implanted dipole(s) is (are) switched on. When they are switched on they appear fixed for the time they are on, disappearing into the changing background shortly afterwards, only to reappear again pointing in the opposite direction as they are switched on in the opposite polarity.

In earlier works the power of distributed current density imaging was demonstrated with computer generated data and analysis of evoked MEG signals and spontaneous activity. Here we have provided some validation for the method, by recovering known details from implanted dipoles in vivo. We emphasize here that the recovery of current dipoles is a most difficult test of distributed source models. We have shown that even in this most unfavourable case the distributed source imaging system we have developed produces, *with minimal a priori assumptions*, a reconstruction, where the large scale spatial features and their temporal variation are easily identified.

References

Balish, M. and Sato, S. Magnetoencephalography in epilepsy research and its perspectives. In: S.J. Williamson, M. Hoke, G. Stroink and M. Kotani (Eds.), Advances in Biomagnetism. Plenum Press, New York, 1989: 269-272.

Balish, M., Sato, S., Connaughton, P. and Kufta, C. Magnetoencephalographic (MEG) localization of multiple subdural electrodes. Neurology, 1991, 41: 1072-1076.

Baumgartner, C. and Deecke, L. Magnetoencephalography in clinical epileptology and epilepsy research. Brain Topogr., 1990, 2: 203-219.

Clarke, C.J.S. and Janday, B.S. Probabilistic methods in a biomagnetic inverse problem. Inverse Problems, 1989, 5: 483-500.

Clarke, C.J.S. Probabilistic methods in a biomagnetic inverse problem. Inverse Problems, 1989, 5: 999-1012.

Clarke, C.J.S., Ioannides, A.A. and Bolton, J.P.R. Localised and distributed source solutions for the biomagnetic inverse problem I. In: S.J. Williamson, M. Hoke, G. Stroink and M. Kotani (Eds.), Advances in Biomagnetism. Plenum Press, New York, 1989: 587-590.

Crowley, C.W., Greenblatt, R.E. and Khalil, I. Minimum norm estimation of current distributions in realistic geometries. In: S.J. Williamson, M. Hoke, G. Stroink and M. Kotani (Eds.), Advances in Biomagnetism. Plenum Press, New York, 1989: 603-606.

Hämäläinen, M.S. and Ilmoniemi, R.J. Interpreting Measured Magnetic Fields of the Brain: Estimates of the Current Distributions. Preprint TKK-F-A559, Helsinki University of Technology, 1984.

Hoke, M., Lehnertz, K., Lutkenhoner, B. and Pantev, C. Cortical auditory evoked magnetic fields: mapping of time and frequency domain aspects. In: K. Mauer (Ed.), Topographic Brain Mapping of EEG and Evoked Potentials. Springer-Verlag, Berlin, 1989: 537-564.

Ioannides, A.A. Comparison of MEG with other functional Imaging Techniques, Clinical Physics and Physiological Measurement Suppl., 1991, A-12, 23-28.

Ioannides, A.A., Bolton, J.P.R., Hasson, R. and Clarke, C.J.S. Localised and distributed source solutions for the biomagnetic inverse problem II. In: S.J. Williamson, M. Hoke, G. Stroink and M. Kotani (Eds.), Advances in Biomagnetism. Plenum Press, New York, 1989a: 591-594.

Ioannides, A.A., Hasson, R. and Bolton, J.P.R. Spatial and Temporal Evolution of Brain Activity. Open University video, July 1989b.

Ioannides, A.A., Bolton, J.P.R. and Clarke, C.J.S. Continuous probabilistic solutions to the biomagnetic inverse problem. Inverse Problems, 1990a, 6: 523-542.

Ioannides, A.A., Hasson, R. and Miseldine, J.G. Model- dependent noise elimination and distributed source solutions for the biomagnetic inverse problem. In: A.F. Gmitro, P.S. Idell and I.J. Lahaie (Eds.), Digital Image Synthesis and Inverse Optics., Proc. SPIE 1351, 1990b: 471-481.

Ioannides, A.A., Singh K.D., Hasson R., Baumann S.B., Rogers R.L., Papanicolaou, A.C., Rogers, R.L., Guinto, F.C. and Papanicolaou, A.C. Comparison of Current Dipole and Magnetic Field Tomography Analyses of the Cortical Response to Auditory Stimuli. Brain Topography 1993 (In press).

Kullman, W.H., Jandt, K.D., Rehm, K., Schlitt, H.A., Dallas, W.J. and Smith, W.E. A linear estimation approach to biomagnetic imaging. In: S.J. Williamson, M. Hoke, G. Stroink and M. Kotani (Eds.), Advances in Biomagnetism. Plenum Press, New York, 1989: 571-574.

Mosher, J.C., Lewis, P.S., Leahy, R., and Singh, M. Multiple Dipole Modelling of Spatio-Temporal MEG Data. In: A.F. Gmitro, P.S. Idell and I.J. Lahaie (Eds.), Digital Image Synthesis and Inverse Optics. Proc SPIE 1351, 1990: 471-475.

Pantev, C., Hoke, M., Lutkenhoner, B. and Lehnertz, K. Tonotopic organisation of the auditory cortex: pitch versus frequency representation. Science, 1986, 244: 486-488.

Papanicolaou, A.C., Baumann, S., Rogers, R.L., Saydjari, C., Amparo, E.G. and Eisenberg, H.M. Localization of auditory response sources using magnetoencephalography and magnetic resonance imaging. Arch. Neurol., 1990, 47: 33-37.

Ribary, U., Ioannides, A.A., Hasson, R., Singh, K.D., Bolton, J.P.R., Lado, F. and Llinas, R. Magnetic Field Tomography (MFT) of Coherent Thalamo-Cortical 40 Hz Oscillations in

Humans, Proc. Nat. Acad. Sci. USA, 1991, 88, 11037-11041.

Rose, D.F., Sato, S., Smith, P.D., Friauf, W. and Ducla-Soares, E. Subdural electrode as a dipole source for magnetoencephalography. Electroenceph. Clin. Neurophysiol., 1989a, 72: 86-90.

Rose, D.F., Ducla-Soares, E., Sato, S., Kufta, C.V. MEG localization of a subdural dipole in a patient. Epilepsia, 1989b, 29: 656-657.

Scherg and Cramon D. von, Two bilateral sources of the late AEP as identified by a spatio-temporal dipole model. Electroenceph. Clin. Neurophysiol. 1985, 62: 32-44.

Scherg, M., Vajsar, J. and Picton, T.W. A source analysis of the late human auditory evoked potentials. J. Cognitive Neuroscience, 1989, 1: 336-355.

Scherg M. Fundamentals of Dipole Source Potential Analysis. In: Auditory Evoked Magnetic Fields and Electric Potentials ed. Grandori, F., Romani, G.L. (Eds), Karger, Basel, 1990, 40-69.

Schmidt R.O. Multiple emitter location and signal parameter estimation. IEEE Trans. Antennas and Propagation, 1986, AP-34: 276-280.

Smith, D.B., Sidman, R.D., Henke, J.S., Flanigin, H., Labiner, D. and Evans, C.N. Scalp and depth recording of induced deep cerebral potentials. Electroenceph. Clin. Neurophysiol., 1983, 55: 145-150.

Smith, D.B., Sidman, R.D., Flanigin, H., Henke, J. and Labiner, D. A reliable method for localizing deep intracranial sources of the EEG. Neurology, 1985, 35: 1702-1707.

Tepley, N., Barkley, G.L., Moran, J.E., Simkins, R.T. and Welch, K.M.A. Observation of spreading cortical depression in migraine patients. In: S.J. Williamson, M. Hoke, G. Stroink and M. Kotani (Eds.), Advances in Biomagnetism. Plenum Press, New York, 1989: 327-330.

Tripp, J.H. Physical Concepts and Mathematical Models. In Biomagnetism: an Interdisciplinary Approach, ed. Williamson, S.J., Romani, G.L., Kaufman, L. and Modena, I., Plenum Press, New York, 1983, 123-139.